Materials Science and Technology Conference and Exhibition 2010, MS and T'10 **4**:2596-2607 01 Dec 2010

Modelling Thermomechanical Behaviour Of Cr-Mo-V Steel

Z. Shi [1], T. J. A. Doel [2], J. Lin [1], P. Bowen [2] and S. Bray [3]

1. Department of Mechanical Engineering, Imperial College London, Exhibition Road, South Kensington, London SW7 2AZ, UK
2. School of Metallurgy and Materials， University of Birmingham，Edgbaston，Birmingham B15 2TT, UK
3. Rolls-Royce plc., PO Box 31, Derby DE24 8BJ, UK

Keywords: Materials modelling, Viscoplasticity, Super CMV

Abstract

This paper presents a mechanism-based approach for modelling the thermomechanical behaviour of a Cr-Mo-V steel. A set of unified viscoplastic constitutive equations were employed to model dislocation density, recrystallisation and grain size during deformation. The evolution of dislocation density accounts for the build-up of dislocations due to plastic strain, the static and dynamic recovery and the effect of recrystallisation. Recrystallisation occurs when a critical dislocation density is reached after an incubation time, and grain size becomes smaller after such event. Gleeble compression tests were used to obtain Stress-strain curves and evaluate the microstructural evolution at different temperature and strain rate, and the material constants for the model were determined from the experimental data.

Introduction

Friction welding is a class of solid state welding processes where heat is generated through mechanical friction between a moving workpiece and a stationary component. Because of its localised weld and the ability to join dissimilar materials, it is finding use in many industries including aerospace industry (such as turbine wheel and shafts). There are many publications related to joining different pairs of dissimilar metals and/or its effect on the microstructures and properties, such as dissimilar steels, nickel based superalloys, Al alloy, Ti alloy, copper, etc [1-6].

Welding process is like a thermomechanical processing operation. During the process, deformation takes place and, depending on strain rate, temperature and initial conditions of the material, various microstructural changes may occur, which, in turn, affects the thermomechanical behaviour of the material. The microstructural changes involves build-up of dislocation density, strain hardening, static and dynamic recovery, recrystallisation and grain growth. These changes are highly temperature and strain rate dependent, and different factors are interacting/competing in the process [7-11].

In recent years, unified approaches have been employed to model interactive effects of microstructural evolution and viscoplastic flow of materials based on continuum theories [12-

15]. In these theories, state variables are introduced to model the evolution of individual microstructural variables (such as grain size, precipitate volume fraction, etc.) during the process, and all these variables contribute to the change in mechanical properties and viscoplastic flow. In this paper, the same approach was applied to a Cr-Mo-V steel – super CMV (SCMV), which has been a candidate material of previous study for inertia welding [1]. A set of unified constitutive equations were established and materials constants in the equations were determined based on the data from experimental work.

Viscoplastic Model

Several material characteristics are changed during thermomechanical processes, including grain size, dislocation density, and recrystallisation, which affect the viscoplastic behaviour of the material. Therefore, grain size, dislocation density, and recrystallised volume fraction are some of the state variables used to model the thermomechanical behaviour.

At a high temperature and a high stress level, deformation process is predominated by dislocation controlled mechanisms and the stress-strain rate relationship is non-linear. Sinh-law is applicable to a wide range of strain rates and stress levels [16], and is used in the current model. Thus the viscoplastic constitutive equation is:

$$\dot{\varepsilon}_{\mathrm{p}} = \mathrm{A}_1 \sinh\left[\mathrm{A}_2(\sigma - \mathrm{R} - \kappa)\right] d^{-\psi_4} \qquad (1)$$

where ε_p is the plastic strain and a dot over a variable represents its time derivative. R represents the isotropic strain hardening of the material, which is directly related to dislocation density. κ is the yield stress and d is the average grain size. A_1 is a temperature dependent material constant, and A_2 and ψ_4 are temperature independent constants.

Equation (1) also shows that the stress consists of three components: the viscoplastic stress, the yield stress and the strain hardening. The strain hardening is caused by the build-up of dislocations and is proportional to the square root of dislocation density [17]. Thus, isotropic strain hardening (R) can be express as

$$R = B_1 \bar{\rho}^{0.5} \qquad (2)$$

where B_1 is a temperature dependent material constant, and $\bar{\rho}$ is a normalised dislocation density.

During deformation, material experiences plastic strain, causing dislocation density to increase and resulting in strain hardening. There are several factors that affect the dislocation density: the development of dislocation density during plastic straining, dynamic recovery of dislocation density during straining, static recovery of dislocation density and the effect of recrystallisation on the evolution of dislocation density. A normalised dislocation density $\bar{\rho} = 1 - \rho_i / \rho$ is used here, where ρ_i and ρ are the initial and current dislocation density in the material [13]. At the beginning, $\bar{\rho}$ has a value of 0 and can increase up to a maximum value of 1 during the deformation process. The rate equation for the normalized dislocation density is

$$\dot{\bar{\rho}} = C_1\left(\frac{d}{d_0}\right)^{\delta_1}\cdot(1-\bar{\rho})\cdot\left|\dot{\varepsilon}_p\right|^{\delta_2} - C_r\cdot\bar{\rho}^{\delta_3} - C_s\frac{\bar{\rho}}{(1-S)^{\delta_4}}\dot{S} \qquad (3)$$

where C_1, C_s, δ_1, δ_2, δ_3 and δ_4 are material constants, C_r is a temperature dependent constant, d_0 is the initial average grain size, S is the recrystallised volume fraction. The first term in Equation (3) models both the development of dislocation density due to plastic strain and dynamic recovery of dislocation density. The dynamic recovery term enables the normalized dislocation density to be limited to the saturated state of dislocation network being 1.0. The second term is due to the static recovery of dislocation density during the thermal process. The third term comes from the contribution of recrystallisation to the recovery of dislocation density.

Recrystallisation is directly related to dislocation density. A critical value of dislocation density is required before recrystallisation can start. $\bar{\rho}_c$ is the critical value of normalised dislocation density, below which recrystallisation will not take place. The value of $\bar{\rho}_c$ is dependent on the temperature. When the normalised dislocation density reaches $\bar{\rho}_c$ at high temperature, given sufficient time, recrystallisation will occur. This time-effect is modelled by an incubation fraction. The recrystallised volume fraction is

$$\dot{S} = H_1\cdot\left[x\cdot\bar{\rho} - \bar{\rho}_c\cdot(1-S)\right]\cdot(1-S)^{\lambda_1} \qquad (4)$$

where λ_1 is a material constant, H_1 is a temperature dependent constant. x is the incubation fraction for the onset of recrystallisation and is dependent on the dislocation density:

$$\dot{x} = X_1\cdot(1-x)\cdot\bar{\rho} \qquad (5)$$

where X_1 is a temperature dependent material constant.

The grain size (d) is affected by the normal grain growth and the refining effect of recrystallisation. Therefore,

$$\dot{d} = G_7\cdot\left(\frac{d_0}{d}\right)^{\psi_1} - G_8\cdot\dot{S}^{\psi_3}\cdot\left(\frac{d}{d_0}\right)^{\psi_2} \qquad (6)$$

where G_8, ψ_1, ψ_2 and ψ_3 are material constants, and G_7 is a temperature dependent material constant.

For the elastic deformation range, Hooke's law of elasticity is applied:

$$\sigma = E\cdot(\varepsilon_T - \varepsilon_p) \qquad (7)$$

where E is Young's modulus, ε_T is the total strain.

Equations (1)-(7) are a set of the unified viscoplastic constitutive equations, describing the evolution of dislocation density, strain hardening, recrystallisation, and grain size. The following expressions were used for the temperature dependant material constants:

$$k = K_0 \cdot \exp\left(\frac{Q_p}{R_g T}\right) \qquad (8a)$$

$$A_1 = A_{10} \cdot \exp\left(\frac{-Q_{a1}}{R_g T}\right) \qquad (8b)$$

$$B_1 = B_{10} \cdot \exp\left(\frac{Q_{b1}}{R_g T}\right) \qquad (8c)$$

$$C_r = C_{r0} \cdot \exp\left(\frac{-Q_r}{R_g T}\right) \qquad (8d)$$

$$G_7 = G_{70} \cdot \exp\left(\frac{-Q_{g7}}{R_g T}\right) \qquad (8e)$$

$$H_1 = H_{10} \cdot \exp\left(\frac{-Q_{h1}}{R_g T}\right) \qquad (8f)$$

$$\bar{\rho}_c = \bar{\rho}_{c0} \cdot \exp\left(\frac{Q_c}{R_g T}\right) \qquad (8g)$$

$$X_1 = X_{10} \cdot \exp\left(\frac{-Q_{x1}}{R_g T}\right) \qquad (8h)$$

where A_{10}, B_{10}, C_{r0}, G_{70}, H_{10}, K_0, Q_{a1}, Q_{b1}, Q_c, Q_{g7}, Q_{h1}, Q_p, Q_r, Q_{x1}, X_{10} and $\bar{\rho}_{c0}$ are constants. R_g is the gas constant, and T is the absolute temperature. These constants were determined by fitting the model results with the experimental data using the same technique detailed in [13].

Material And Experiments

The material used in the study is a high strength low alloy Cr-Mo-V steel – super CMV (SCMV). The composition of SCMV is Fe-0.3C-3.15Cr-1.6Mo-0.1V-0.6Si (wt%).

Compression tests were carried out using Gleeble machine. The dimensions of the testpieces were cylindrical shape with a diameter of 8 mm and a length of 12 mm. Stress-strain curves were obtained for different temperatures and/or different strain rates. The average grain sizes of the tested specimens were analysed and reported elsewhere [18]. Experimental results were used to determine the material constant of the viscoplastic constitutive equations.

Results And Discussions

From Equation (8a), it follows that

$$\ln(\kappa) = \ln(K_0) + \frac{Q_p}{R_g}\frac{1}{T}. \qquad (9a)$$

The half of the flow stresses ($\sigma/2$) for each temperature at a strain of 0.1 and a strain rate of 1 s^{-1} are plotted in Fig. 1. It shows that $\ln(\sigma/2)$ is linearly proportional to the value of 1/T. This is taken as the yield stress κ. By matching Equation (9a) with the fitting in Fig. 1, one obtains

$$\kappa = 0.372 \cdot \exp\left(\frac{53900}{R_g T}\right). \tag{9b}$$

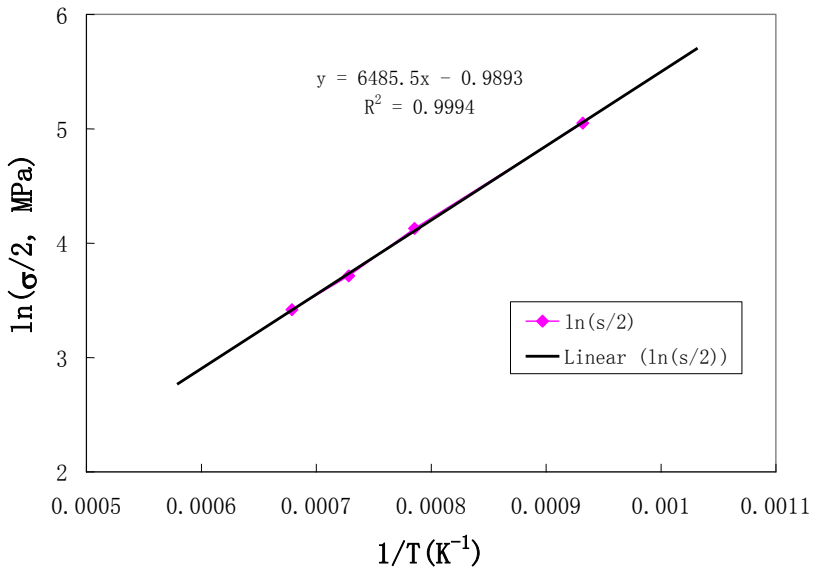

Fig. 1 Relationship of flow stress (σ) at 0.1 strain and 1 s^{-1}strain rate with temperature - experimental results and linear fitting.

The Young's modulus expression was obtained by fitting the available data during heating [19] and extrapolated to the whole temperature range. Fig. 2 shows the values of Young's modulus at different temperature and the trend fitting equation. An additional point has been added at 1973 K so that it will not become negative for any possible modelling temperature range during inertia welding. The final equation used in the model for Young's modulus (MPa) is

$$E = 223000 - 26.24T - 0.04403T^2. \tag{10}$$

The material constants were determined after comparing the simulation results with the Gleeble test data. Table 1 lists the final values for the material constants used in the viscoplastic model for SCMV.

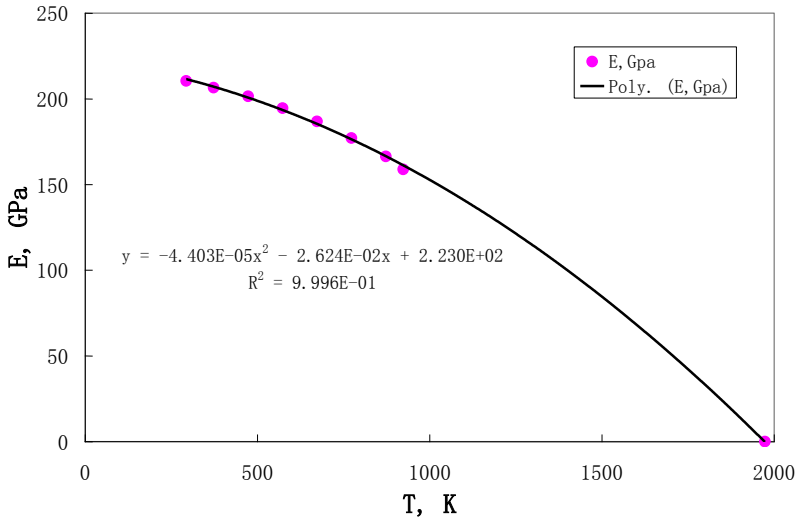

Fig. 2 Young's modulus of SCMV

Table 1 Material constants used in SCMV model

A_{10}	A_2	B_{10}	C_1	C_{r0}	C_s
550	0.1	0.49	1.2	2.65×10^4	1
G_{70}	G_8	H_{10}	k_0	Q_{a1}	Q_{b1}
1.23×10^8	28	2.48×10^5	0.372	5×10^4	6×10^4
Q_c	Q_{g7}	Q_{h1}	Q_p	Q_r	Q_{x1}
4.5×10^4	2×10^5	1.1×10^5	5.39×10^4	9.5×10^4	8×10^4
X_{10}	ρ_{c0}	δ_1	δ_2	δ_3	δ_4
1.3×10^6	0.0022	1	1.2	1.88	1
ψ_1	ψ_2	ψ_3	ψ_4	λ_1	d_0
2	0.12	1	0.5	1	19.5 μm

Figs. 3 and 4 show the modelling results up to a strain of 0.5 for temperatures of 1273, 1373, 1473 and 1573 K at a strain rate of 1 s^{-1}, together with the experimental stress-strain curves. The temperature history in Fig. 3 shows that the testpiece is first heated at 20 $K.s^{-1}$ to the compression test temperature, held for 1 s before starting the compression test, then cooled at 50 $K.s^{-1}$. This cooling rate is approximated from the natural cooling tests. The cooling period is included here for the purpose of simulating the final grain size. Simulation was stopped when the temperature was cooled to 1073 K as further cooling has insignificant effect on the grain size. From Fig. 3, it can be seen that normal grain growth takes place during heating, but only becomes obvious after 1100 K. As the temperature increases, the grain growth rate becomes larger. For a particular temperature, however, Equation (4) indicates that the growth rate decreases with increasing grain size and a saturated state of grain size may be reached after some time. Fig. 3 also shows that there is a sudden drop in grain size, which is caused by recrystallisation. After recrystallisation, the grains start to grow again. The growth rate is faster at first, then gradually grain growth comes to a plateau. The main reason for this is that the temperature is decreasing after deformation, therefore reducing the mobility of the atoms.

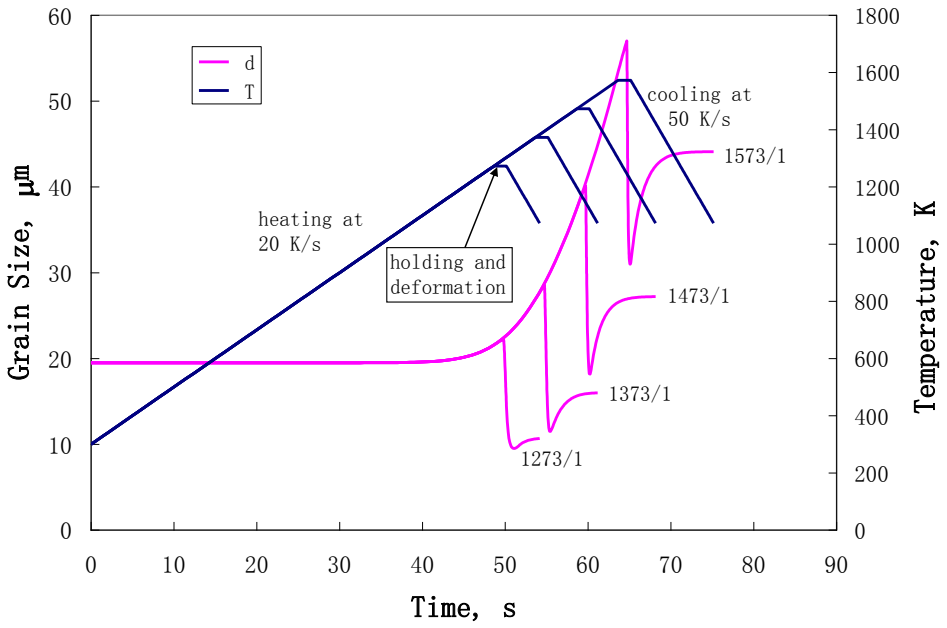

Fig. 3 Simulation thermal history and change is grain size for different testing temperatures. In the figure, xxxx/x (e.g., 1473/1) indicates the temperature in K and strain rate in s^{-1} for the test.

As shown in Fig. 4, a good match for the stress-strain curves has been achieved. The flow stress first increases with the strain because the dislocation density is increased as is the strain hardening effect. Then recrystallisation occurs, reducing the dislocation density, the flow stress and also the grain size. The vertical parts of the curves at $\varepsilon = 0.5$ are the results from the cooling period when no more load was applied (see Fig. 3 for comparison). Fig. 4 shows that as the test temperature increases, the flow stress becomes lower, incubation period becomes shorter, and recrystallisation process becomes faster. From the graph of recrystallised volume fraction, it can be seen that some recrystallisation may continue when deformation ends.

The effects of the test temperature and the strain rate on the grain sizes are plotted in Figs. 5 and 6 respectively. The experimental data are from Ref. [18]. As can be seen from the figures, the grain size increases with testing temperature due to higher activity/diffusion coefficient at higher temperature. The simulation results of the temperature effect on the grain size compare favourably with the experimental data. For the effect of strain rate at 1473 K, the grain size prediction from the current model is higher than the experimental results, especially at the strain rate of 0.1 s^{-1}.

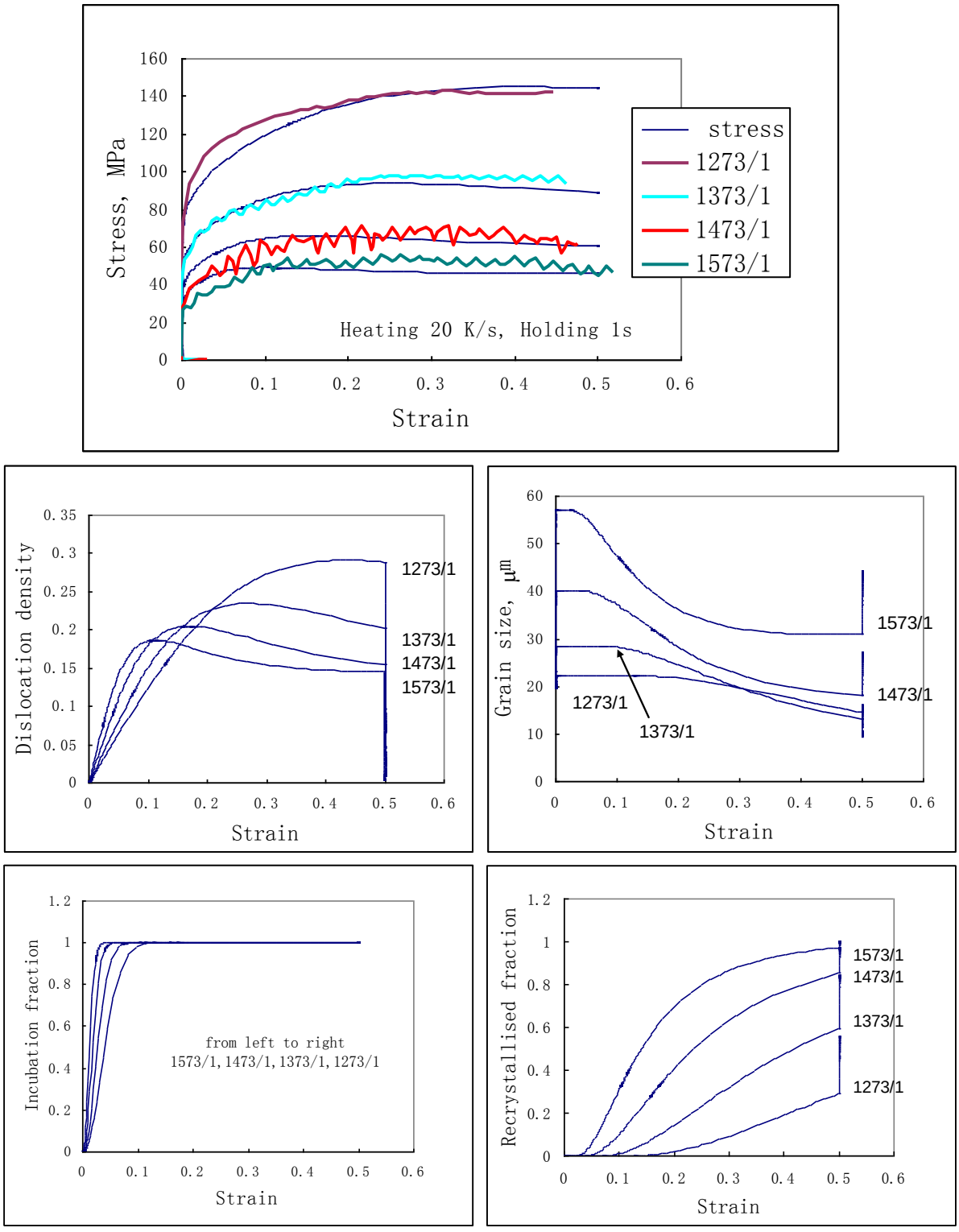

Fig. 4 Effect of temperature on the flow stress, dislocation density, grain size, incubation fraction and recrystallised volume fraction of SCMV, at strain rate of 1 s^{-1}.

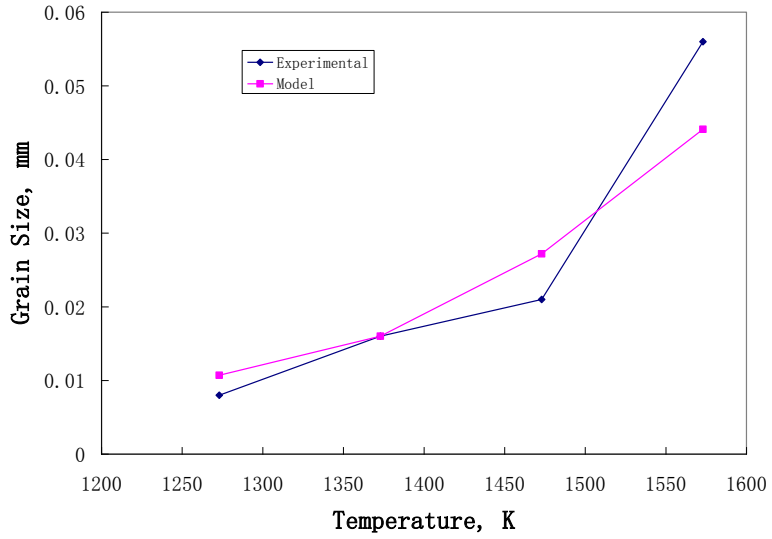

Fig. 5 Effects of test temperature on the grain size of SCMV after compression test at 0.5 strain and 1 s^{-1} strain rate.

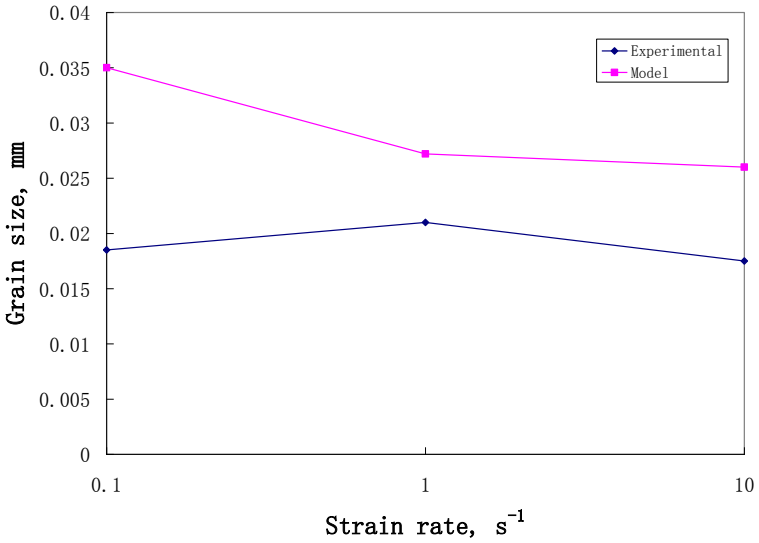

Fig. 6 Effect of strain rate on the grain sizes of SCMV after compression test at 1473 K and 0.5 strain.

Fig. 7 shows the effect of strain rate on the viscoplastic behaviour of SCMV at 1473K. The model results for the flow stress are in good agreement with the experimental data. The higher the strain rate, the higher the normalised dislocation density and the flow stress. For higher strain rate, the incubation period comes to completion at higher strain. The effect of strain rate on the recrystallisation and the grain size is not straightforward but varies depending on the test temperature. This is because that recrystallisation depends on dislocation density, temperature, and time. At the strain of 0.5, the strain rate of 0.1 s^{-1} has the most recrystallised volume fraction at 1473 K.

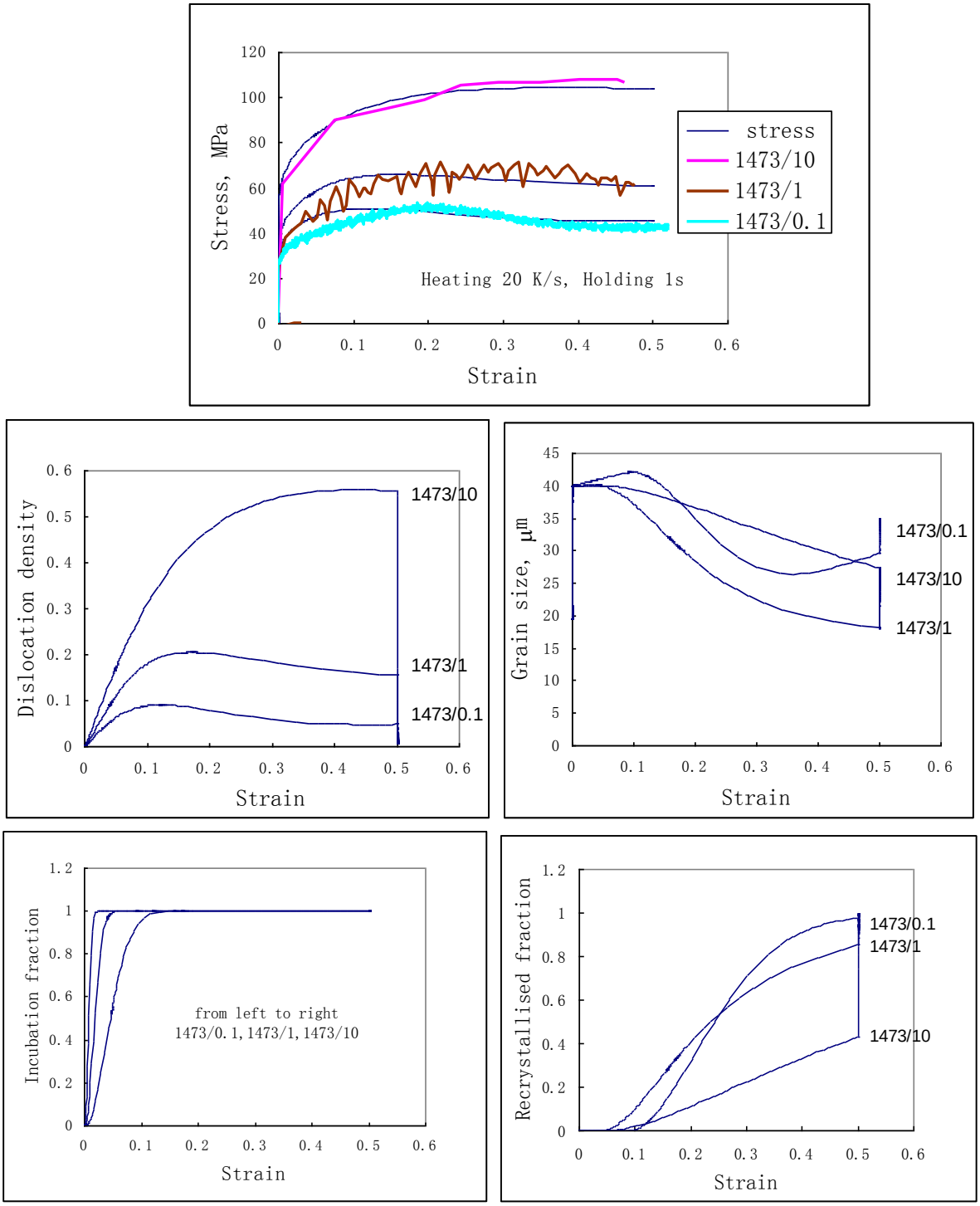

Fig. 7 Effect of strain rate on the viscoplastic behaviour of SCMV at 1473 K.

However, results may look different if it is plotted as a function of time rather than strain. For a certain strain, higher strain rate means higher dislocation density, but less time for any process to proceed. In Fig. 7, for example, recrystallisation advances fastest as a function of strain for the lowest strain rate of 0.1 s^{-1}. However, from time point of view, recrystallisation is

slowest at this strain rate, as shown in Fig. 8. When recrystallisation occurs, the grain size has two competing factors: normal grain growth and refinement through recrystallisation. In Fig. 8, the result of 0.1 s^{-1} shows that the grain size first increases through normal grain growth, then decreases because of recrystallisation, and it starts to grow again when recrystallisation becomes nearly completed and normal grain growth has a stronger effect over recrystallisation.

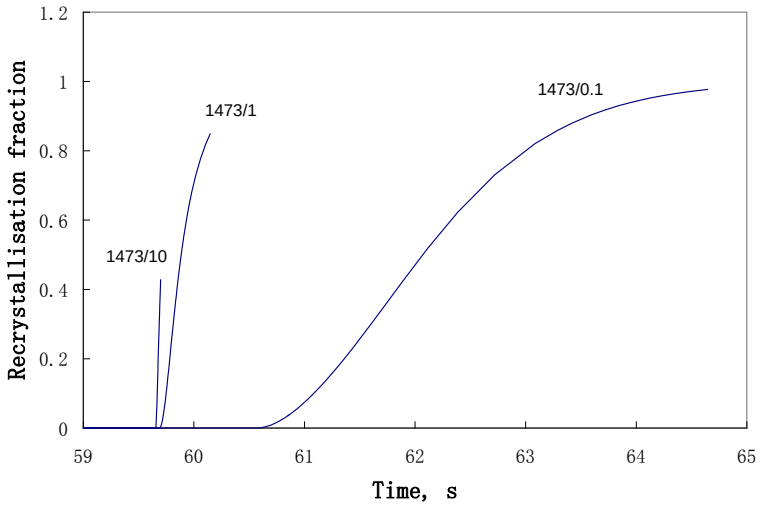

Fig.8 Effect of strain rate on the recrystallisation of SCMV at 1473 K, as a function of time.

Conclusions

A material model for the viscoplastic behaviour has been developed for a Cr-Mo-V steel, super CMV. Material constants for the equations have been determined. Simulated flow stresses are in good agreement with the experimental ones in the temperature range studied. The flow stress increased with decreasing temperature and increasing strain rate. Recrystallisation occurred in the process, while grain size was refined and dislocation density decreased after such event. The modelled grain sizes are in fair agreement with experimental results.

Acknowledgments

This work has been carried out under the PROMOTE project funded by The Technology Strategy Board. The Technology Strategy Board is a business-led executive non-departmental public body, established by the government. Its mission is to promote and support research into, and development and exploitation of, technology and innovation for the benefit of UK business, in order to increase economic growth and improve the quality of life. It is sponsored by the Department for Innovation, Universities and Skills (DIUS). Please visit www.innovateuk.org for further information.

References

[1] R. Moat, M. Karadge, M. Preuss, S. Bray, and M. Rawson, Phase transformations across high strength dissimilar steel inertia friction weld, *J. Mater. Process. Tech.*, Vol. 204, 2008, p. 48–58.

[2] Z.W. Huang, H.Y. Li, M. Preuss, M. Karadge, P. Bowen, S. Bray, and G. Baxter: Inertia friction welding dissimilar nickel-based superalloys alloy 720Li to IN718, *Metall. Mater. Trans. A – Phys. Metall. Mater. Sci.*, Vol. 38A (7), 2007, p. 1608-1620.

[3] Chen, YC; Nakata, K, Microstructural characterization and mechanical properties in friction stir welding of aluminum and titanium dissimilar alloys, *Mater. Design*, 2009, Vol. 30 (3), p. 469-474.

[4] S. Celik, and I. Ersozlu, Investigation of the mechanical properties and microstructure of friction welded joints between AISI 4140 and AISI 1050 steels, *Mater. Design*, Vol. 30 (4), 2009, p. 970-97.

[5] J. Ouyang, E. Yarrapareddy, and R. Kovacevic, Microstructural evolution in the friction stir welded 6061 aluminum alloy (T6-temper condition) to copper, *J. Mater. Process. Tech.*, Vol. 172, 2006, p. 110-122.

[6] Watanabe, T; Takayama, H, Yanagisawa, A, Joining of aluminum alloy to steel by friction stir welding, *J. Mater. Process. Tech.*, Vol. 178 (1-3), 2006, P. 342-349.

[7] C.M. Sellars, Modelling microstructural development during hot rolling, *Mater. Sci. Technol.*, Vol. 15, 1990, p. 1072-1081.

[8] E. Busso, A continuum theory of dynamic recrystallisation with microstructure-related length scales, *Int. J. Plast.*, Vol. 14 (4-5), 1999, p. 319-353.

[9] R. Colas, A model of the hot deformation of low carbon steel, *J. Mater. Process. Tech.*, Vol. 62, 1996, p. 180-184.

[10] C. Roucoules, and P.D. Hodgson, Post-dynamic recrystallisation after multiple peak dynamic recrystallisation in C-Mn steels, *Mater. Sci. Technol.*, Vol. 11, 1995, p. 548-555.

[11] T. Sakai, and J.J. Jonas, Overview no. 35: dynamic recrystallisation: mechanical and microstructural considerations, *Acta Metall.*, 32 (2), 1984, p.189-209.

[12] J. Lin, and Y. Liu, A set of unified constitutive equations for modelling microstructure evolution in hot deformation. *J. Mater. Process. Tech.*, Vol. 143, 2005, p. 281–285.

[13] J. Lin, Y. Liu, D. C. J. Farrugia, And M. Zhou (2005): Development of dislocation-based unified material model for simulating microstructure evolution in multipass hot rolling, *Phil. Mag.*, Vol. 85 (18), 2006, p. 1967–1987.

[14] R.P. Garrett, J. Lin, and T.A. Dean, An investigation of the effects of solution heat treatment on mechanical properties for AA 6xxx alloys: experimentation and modeling, *Int. J. Plast.*, Vol. 21, 2005, p. 1640–1657.

[15] H. Li, J. Lin, T.A. Dean, S.W. Wen, A.C. Bannister, Modelling mechanical property recovery of a linepipe steel in annealing process, *Int. J. Plast.*, Vol. 25, 2009, p. 1049–1065.

[16] H.J. Frost and M.F. Ashby, *Deformation-Mechanism Maps*, Pergamon Press, Oxford, 1982.

[17] Y. Estrin, Dislocation theory based constitutive modelling: foundations and applications, *J. Mater. Process. Tech.*, Vol. 80–81, 1998, p. 33–39.

[18] S. Bray and A. Palfryema, Prior Austenite grain size measurement of Aermet-100 and Super-CMV compression samples, *Rolls Royce Plc Internal Report*, May 2010.

[19] C.J. Bennett, *Inertia Friction Welding of High Strength Aerospace Alloys*. PhD Thesis, the University of Nottingham, Nottingham, 2007.